Remotely triggered microearthquakes and tremor in central California following the 2010 M_w 8.8 Chile earthquake

Zhigang Peng,[1] David P. Hill,[2] David R. Shelly,[2] and Chastity Aiken[1]

Received 13 September 2010; revised 28 October 2010; accepted 2 November 2010; published 31 December 2010.

[1] We examine remotely triggered microearthquakes and tectonic tremor in central California following the 2010 M_w 8.8 Chile earthquake. Several microearthquakes near the Coso Geothermal Field were apparently triggered, with the largest earthquake (M_l 3.5) occurring during the large-amplitude Love surface waves. The Chile mainshock also triggered numerous tremor bursts near the Parkfield-Cholame section of the San Andreas Fault (SAF). The locally triggered tremor bursts are partially masked at lower frequencies by the regionally triggered earthquake signals from Coso, but can be identified by applying high-pass or matched filters. Both triggered tremor along the SAF and the M_l 3.5 earthquake in Coso are consistent with frictional failure at different depths on critically-stressed faults under the Coulomb failure criteria. The triggered tremor, however, appears to be more phase-correlated with the surface waves than the triggered earthquakes, likely reflecting differences in constitutive properties between the brittle, seismogenic crust and the underlying lower crust.
Citation: Peng, Z., D. P. Hill, D. R. Shelly, and C. Aiken (2010), Remotely triggered microearthquakes and tremor in central California following the 2010 M_w 8.8 Chile earthquake, *Geophys. Res. Lett.*, *37*, L24312, doi:10.1029/2010GL045462.

1. Introduction

[2] Recent studies have shown that large earthquakes can dynamically trigger microearthquakes and deep tectonic tremor thousands of kilometers away [e.g., *Hill and Prejean*, 2007; *Peng and Gomberg*, 2010, and references therein]. While dynamic triggering was mostly observed in extensional regimes and geothermal/volcanic systems [*Hill and Prejean*, 2007, and reference therein], recent studies found that dynamic triggering could also occur in other tectonic environments not associated with geothermal/volcanic regions [e.g., *Velasco et al.*, 2008; *Jiang et al.*, 2010]. In particular, both the Love and Rayleigh waves can trigger microearthquakes [*Velasco et al.*, 2008; *Jiang et al.*, 2010] and tremor [*Rubinstein et al.*, 2009; *Peng et al.*, 2009], and many (but not all) instances of triggering are consistent with a Coulomb failure criteria, which is a function of wave type, amplitude, frequency and incident angles [*Hill*, 2010].

[3] Most triggered microearthquakes occur within the brittle seismogenic zone in the upper crust, while triggered tremor is generally located in the more ductile lower crust below the seismogenic zone. It is not clear whether a common physical model can explain both observations. In this study, we examine triggered microearthquakes and tremor in central California (Figure 1) following the M_w 8.8 earthquake that occurred offshore Maule, Chile on 2010/02/27. In particular, we identify triggered microearthquakes in the Coso Geothermal Field (CGF), a transtensional tectonic regime at the southern end of the Owens valley. This is one of the most seismically active regions in California [*Bhattacharyya and Lees*, 2002], and is repeatedly triggered by large regional and teleseismic earthquakes [e.g., *Prejean et al.*, 2004]. In addition, we identify triggered deep tremor and low-frequency earthquakes (LFEs) around the Parkfield-Cholame section of the San Andreas Fault (SAF), where both ambient and triggered tremor has been found [e.g., *Nadeau and Guilhem*, 2009; *Peng et al.*, 2009]. It has been argued that tremor reflects shear failure at the plate interface and is composed of many LFEs [*Shelly et al.*, 2007]. However, it remains to be tested whether this is the case for triggered tremor. In the following sections, we first describe the observations in both regions, followed by an analysis of triggering potential based on the Coulomb failure criteria. Finally, we propose a common mechanism to explain dynamic triggering in both regions.

2. Triggered Earthquakes in the Coso Geothermal Field

[4] We identify earthquakes around the CGF associated with the Chile mainshock by examining both the Southern California Seismic Network (SCSN) earthquake catalog (see auxiliary material) and continuous waveform recordings.[1] Four microearthquakes with $M_l \geq 2$ are listed in the SCSN catalog within 1 hr of the predicted P wave arrival from the Chile earthquake (Figures 1a and 2a). They occurred at shallow depth (<3 km) and clustered in space. The largest of these, an M_l 3.5 event, occurred during the large-amplitude 200-s mantle Love wave pulse (Figure 2b) recorded by the broadband station JRC2 ~12 km SE of the epicenter (Figure 1a). This compares with only two $M_l < 2$ events during the six hours prior to the Chile mainshock. Three high-frequency bursts during the teleseismic waves from the Chile mainshock are clearly visible in the unfiltered broadband seismogram from JRC2 (Figure 2b), and the 2–16 Hz band-pass filtered seismogram reveal four high-frequency bursts with times corresponding to the four local earthquakes listed in the SCSN catalog (Figure 2c). The spectrogram plot reveals three additional, but weaker, high-frequency bursts (Figure 2d).

[5] Because the CGF is seismically active, it is possible that the earthquakes during the wavetrain of the Chile

[1]School of Earth and Atmospheric Sciences, Georgia Institute of Technology, Atlanta, Georgia, USA.
[2]U.S. Geological Survey, Menlo Park, California, USA.

0094-8276/10/2010GL045462

[1]Auxiliary materials are available in the HTML. doi:10.1029/2010GL045462.

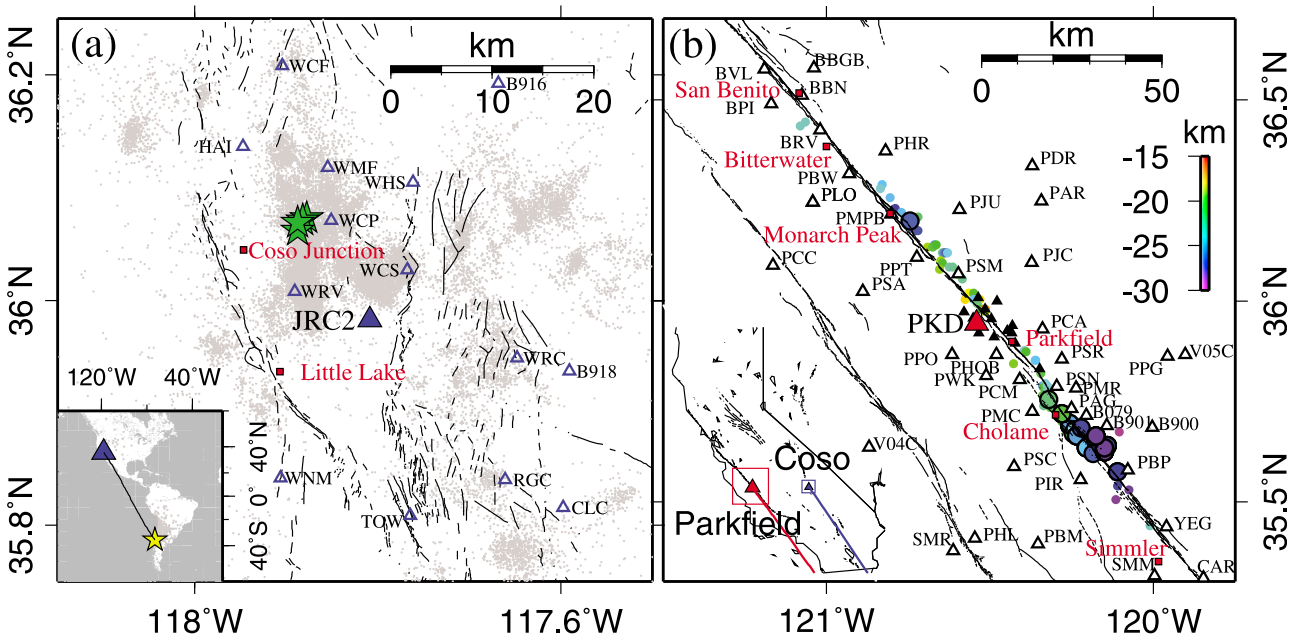

Figure 1. The study region in central California. Inset shows the epicenter of the 2010 Mw 8.8 Chile mainshock (yellow star), the study areas (blue triangle), and the great circle ray path. (a) Map view of the Coso Geothermal Field. Seismic stations belonging to the SCSN are denoted as blue triangles. Gray dots signify earthquakes since 1999 listed in the SCSN catalog. Green stars represent four earthquakes that occurred during the wavetrain of the 2010 M_w8.8 Chile mainshock. (b) Map view of Parkfield section of San Andreas Fault. Seismic stations of the HRSN and the broadband station PKD are denoted by black triangles and red triangle, respectively. The rest seismic stations are denoted by white triangles with selected station names marked. Low frequency earthquakes from *Shelly and Hardebeck* [2010] are represented as circles color-coded by depth, with larger circles indicating those triggered by the 2010 M_w8.8 Chile mainshock.

mainshock could be due to random coincidence. We test the hypothesis that these events are triggered by the Chile mainshock by computing the commonly used β-statistic value [*Kilb et al.*, 2002] and estimating the likelihood of seeing an $M_l \geq 3.45$ event and 4 $M_l \geq 2$ events within 1 hr occurring by random chance. The β-values with different time windows before the mainshock and 1 hr after the predicted arrival of the *P* wave are all larger than 2, and we can reject the hypothesis that these events occur by random chance at the 99% confidence level (auxiliary material and Figure S1). On the other hand, if we keep the pre-mainshock time window as 15 day and increase the post-mainshock time window to 15 day, the β-value decreases to 1.75, suggesting that the seismicity increase following the Chile mainshock is statistically significant only within a short time window.

3. Triggered Tremor and LFEs Along the San Andreas Fault

[6] Similarly, we search for evidence of triggered tremor along the Parkfield-Cholame section of the SAF by the following two methods: (1) a matched-filter technique with 88 LFE waveform templates [*Shelly and Hardebeck*, 2010] and (2) visually with high-pass-filtered continuous waveforms in this region. Figure 2e shows a swarm of LFEs immediately after the predicted arrivals of the Love wave at the broadband station PKD. These LFEs mostly occurred ~30 km south of Parkfield near Cholame (Figure 1b), where the majority of the strong tremor and LFEs are located [*Nadeau and Guilhem*, 2009; *Peng et al.*, 2009; *Shelly and Hardebeck*, 2010]. We also calculate the β-value with different time windows and verify that the triggering is statistically significant (auxiliary material).

[7] In the second approach, we examine continuous waveforms recorded at nearby surface and borehole stations. The transverse-component broadband seismogram recorded at station PKD (Figure 2f) shows a clear Love wave phase, similar to that at station JRC2 (Figure 2b). The largest signal shown in the 2-16 Hz band-pass-filtered seismogram at the nearby borehole station GHIB occurs around the second half-cycle of the Love wave (Figures 2g and 3c), and has two peaks of seismic energy and tremor-like characteristics. A close examination of this and a similar signal around the teleseismic *S* wave reveals that they are generated by sources outside the study area (Figure S2). Indeed, they match the predicted *P* and *S* waves from the earthquakes that are triggered near Coso by the Chile event (Figure S3). In addition, the associated signals are generally below 15 Hz (Figure 2h), which is also consistent with an epicentral distance of ~240 km to the station PKD.

[8] We note the absence of LFE detections within the first two cycles of the Love waves (Figures 2g and 3d). This is likely because the LFE detection was done in the 2-8 Hz band, which contains a mixture of locally triggered tremor and regional earthquake signals from Coso. To suppress the regional earthquake signals, we apply a higher band-pass filter of 15-30 Hz [*Guilhem et al.*, 2010]. As shown in Figure 3d, clear tremor signals are shown in this band and correlate well with the first few peaks of the Love wave.

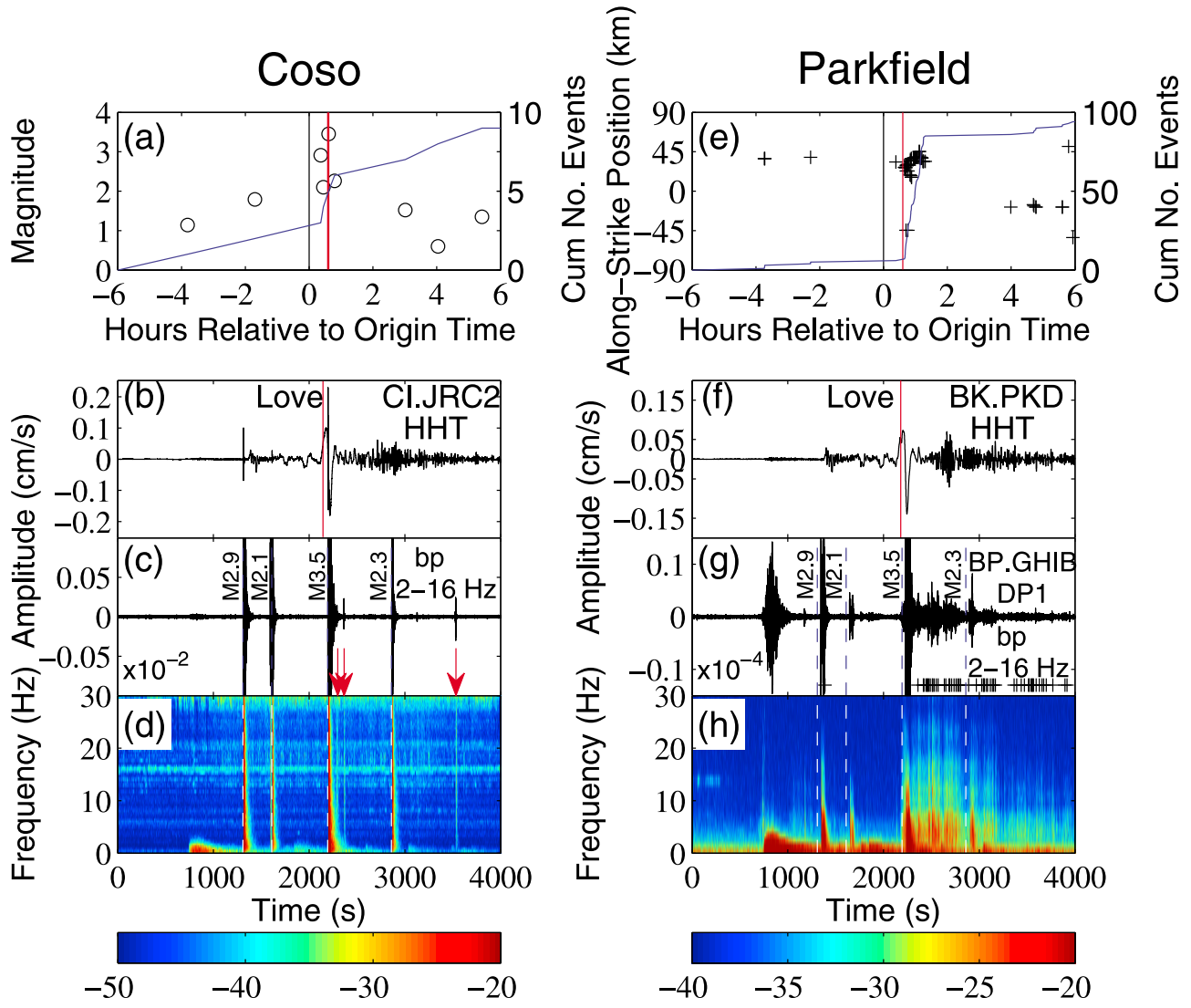

Figure 2. (a) Magnitudes versus occurrence times of microearthquakes around Coso within 6 hours of the origin time of the 2010 Chile mainshock. The red line marks the Love wave arrival with the velocity of 4.3 km/s. The blue line shows the cumulative numbers of events. (b) Instrumented-corrected transverse-component seismogram recorded at station JRC2, (c) 2–16 Hz band-pass-filtered seismogram, and (d) the corresponding spectrogram showing teleseismic signals of the Chile earthquake and 4 local earthquakes with their magnitudes marked in Figure 2c. (e) Along-strike distances versus occurrence times of low-frequency earthquakes (LFEs) around Parkfield within 6 hours relative to the origin time of the 2010 Chilean earthquake. The blue line shows the cumulative numbers of LFEs. (f) Instrumented-corrected transverse-component seismogram recorded at station PKD, (g) 2–16 Hz band-pass-filtered seismogram recorded at GHIB, and (h) the corresponding spectrogram showing teleseismic signals of the Chile mainshock, regional earthquakes near Coso and locally tremor signals. The occurrence times of the LFEs are marked as crosses in Figure 2g.

Similar tremor signals are also shown at later times and appear to be modulated by the Rayleigh waves (Figures 3d and S4).

4. Triggering Potential

[9] Here we evaluate the relative triggering potential of the 200-s Love and Rayleigh waves as a function of incidence angle on critically stressed faults under the Coulomb failure (CF) criteria following the approach described by *Hill* [2010] with results summarized in Figure 4. The focal mechanism for the M_l 3.5 Coso earthquake is not well resolved. The results in Figure 4a are based on our assumption that the M_l 3.5 event occurred on a nearby vertical, north-striking, dextral strike-slip fault, consistent with the conjugate faulting style in this section of the Coso region [*Bhattacharyya and Lees*, 2002]. For an incidence angle, γ = 35°, and an assumed apparent friction coefficient μ^* = 0.4, the Love wave potential is ~1.9 times that of the Rayleigh wave potential, and our estimate of the peak CF dynamic stresses on the fault surface at 2 km depth is 2.9 and 1.5 kPa, respectively. See auxiliary material and Figure S5 for analogous results for three alternate focal mechanisms determined for the M_l 3.5 event, all of which have lower triggering potentials than the vertical fault in Figure 4a.

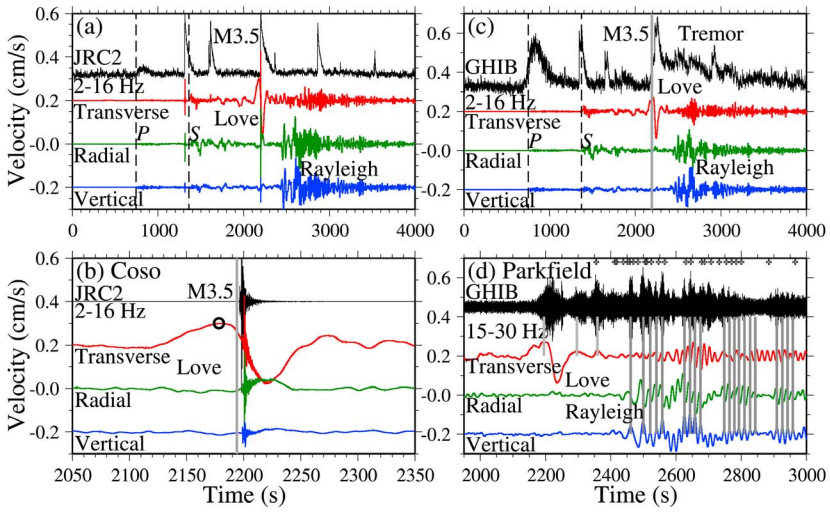

Figure 3. (a) Instrument-corrected three-component velocity seismograms recorded at station JRC2 near Coso plotted together with the smoothed 2–16 Hz band-pass-filtered envelope function. (b) A zoom-in plot of Figure 3a showing the correlations between the Love wave and the M_l 3.5 event, with its origin time marked by the vertical gray line. (c) Instrument-corrected three-component velocity seismograms recorded at station PKD near Parkfield plotted together with the smoothed 2–16 Hz band-pass-filtered envelope function at station GHIB. The origin time of the M_l 3.5 event near Coso is marked by the vertical gray line. (d) A zoom-in plot showing the correlations between the surface waves of the Chile mainshock and local tremor signals in the 15–30 Hz band. The occurrence times of the LFEs are marked as crosses. The peaks of the Love and Rayleigh waves are marked by gray vertical lines. All the traces have been time shifted to reflect their relationship at the tremor source region (auxiliary material).

[10] The Chile surface waves have nearly strike-parallel incidence on the Parkfield section of the SAF with an assumed friction coefficient, $\mu^* = 0.2$, such that the Coulomb failure triggering potential for Love and Rayleigh waves is near-maximal and -null, respectively (Figure 4b). Estimated peak CF dynamic stresses on the fault at 25 km depth are 3.2 and 0.07 kPa for Love and Rayleigh waves, respectively. Note, however, that although the Rayleigh wave CF potential for inducing strike-parallel shear slip is minimal, the Rayleigh wave dilatational stress component, $\delta\Delta$ for this incidence angle is ~3 times the normal stress component, $\delta\sigma_n$. Under fluid-saturated, undrained conditions, this admits a possible mechanism for Rayleigh-wave modulation of tremor triggered by the earlier arriving Love wave through pore-pressure fluctuations on the fault plane (see Hill, 2010). The results are similar for apparent friction coefficients ranging from $\mu^* = 0.0$ to 0.6 (see auxiliary material and Figure S6).

5. Discussion

[11] At least 4 microearthquakes at shallow depth (< 3 km) in the CGF were likely triggered by teleseismic waves from the Chile earthquake. The largest, an M_l 3.5 event, occurred during the pronounced 200-s mantle Love wave pulse. Although the associated slip-parallel dynamic stresses are small (~3 kPa), the observation is consistent with a higher Coulomb-failure triggering potential for Love waves than for Rayleigh waves incident on the likely source fault for this earthquake (Figure 4). This underscores that, depending on incidence angles with respect to fault orientation, Love waves are capable of triggering local seismicity in geothermal/volcanic areas by simple Coulomb failure as well as the more commonly reported triggering by Rayleigh waves [*Hill and Prejean*, 2007]. We note that only the M_l 3.5 event matches with this model prediction, and the other events either occur during the teleseismic body waves, or immediately after the passage of large-amplitude surface waves (Figure S7). Because the likelihood of having 4 $M_l \geq 2$ earthquakes in any given hr is relatively low (<1%), however we still consider them as triggered by either the teleseismic body [e.g., *Miyazawa et al.*, 2005; *Ghosh et al.*, 2009] or surface waves, but with some time delays between the dynamic waves and triggered seismicity [e.g., *Hill and Prejean*, 2007].

[12] Removing signals from the Coso earthquakes on the SAF seismograms by applying a higher band-pass-filter (15–30 Hz) reveals that SAF tremor was clearly triggered when the Love wave particle velocity from the Chile earthquake is to the southwest (positive) direction (Figure 3d), exciting right-lateral shear stresses. This is consistent with recent observations [*Peng et al.*, 2009] and modeling of triggered tremor [*Hill*, 2010] in this and other regions. We can rule out the possibility of the M_l 3.5 Coso event initiating the SAF tremor because the tremor signals between 15–30 Hz appeared earlier than the regional earthquake signals at 2–16 Hz (Figure S8).

[13] We also identified many LFEs during the triggered tremor episodes as well as apparent modulation of tremor during the 20–30 s Rayleigh wave coda (Figure 3d), which may reflect a role for the Rayleigh wave dilatational stress (Figure 4b). These observations suggest that triggered tremor likely reflects shear failure on the deep extension of the SAF, similar to ambient tremor observed in the same region [*Shelly and Hardebeck*, 2010].

[14] Our observations suggest that the frictional shear failure under the Coulomb criterion may explain at least

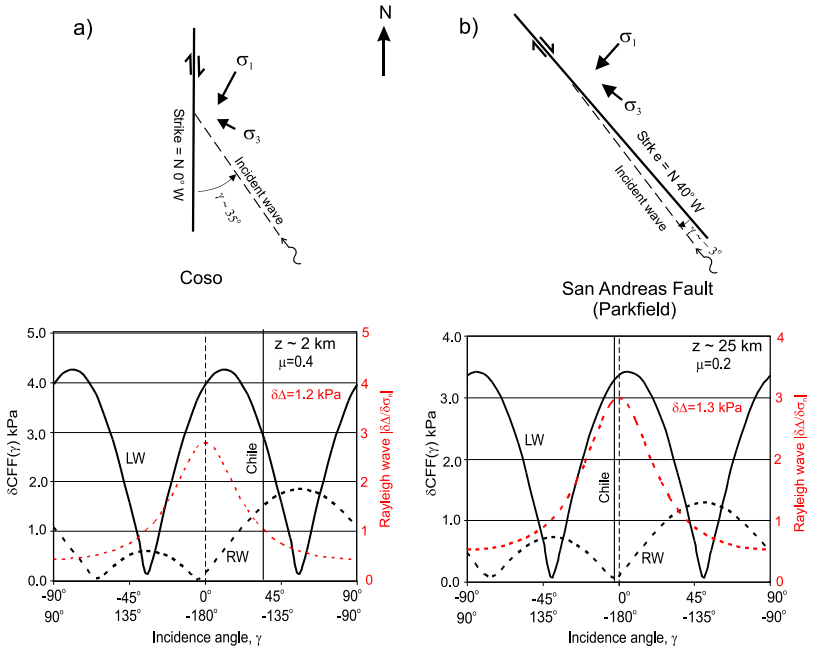

Figure 4. Triggering potential for 200-s Love and Rayleigh waves from the M_w 8.8 Chile earthquake for incidence on (a) a vertical, strike-slip fault in the Coso Geothermal Field at a depth of $z \sim 2$ km, and (b) the Parkfield-Cholame section of the San Andreas Fault (SAF) at a depth of $z \sim 25$ km. The upper diagrams are map views showing local orientation of the fault traces (heavy lines), the surface wave incidence angles, γ, from the Chile earthquake, and the approximate orientations for the regional greatest and least principal stresses, σ_1 and σ_3, respectively from *Feng and Lees* [1998] and *Townend and Zoback* [2004]. The lower diagrams show the triggering potential in terms of the dynamic Coulomb-failure stress, δCF(γ) for Love (LW, solid line) and Rayleigh (RW, dashed line) waves as defined by *Hill* [2010] for assumed apparent friction coefficients, $\mu^* = 0.4$ and 0.2 for Coso and the SAF, respectively. The ratio of the RW dilatational-to-normal stress, $|\delta\Delta/\sigma_n|$ (dashed red line) is a measure of the potential of the RW dilatational stress component to modulate triggered activity with potential increasing with increasing values > 1. Note that $\delta\Delta$ is isotropic and independent of the incidence angle γ [*Hill*, 2010]. The δCF(γ) stresses at 25 km are based on observed transverse and vertical peak displacement amplitudes for 200-s surface waves of 3.7 and 1.3 cm on station JRC2 at Coso (Figure 4a) and 1.4 and 3.0 cm at station PKD along the SAF near Parkfield (Figure 4b).

some shallow earthquakes and most deep tremor and LFEs triggered by surface waves with peak dynamic stresses on the order of a few kPa. The deep tremor and LFEs appear to be well modulated by the surface waves (Figure 3d), indicating a near instantaneous response to the dynamic stresses. However the relationship between the triggered earthquakes and teleseismic waves in the seismogenic crust is variable. The M_l 3.5 event in Coso occurred during the large-amplitude Love wave pulse while other events show no clear correlations with any particular teleseismic wave phase. In addition, the origin time of the M_l 3.5 event lags the peak of the Love wave velocity (a proxy for peak shear stress) by about 16 s (Figure 3b). These observations may reflect inherent difference in constitutive properties between the brittle, seismogenic crust and the underlying transition zone at depths of 20–30 km that host tectonic tremor, as well as different nucleation-time and processes for shallow earthquakes and deep tremor. This is an important topic to be pursued in subsequent studies.

[15] **Acknowledgments.** We thank Wei-Chuang Huang at the Naval Weapons Laboratory at China Lake and Wenzheng Yang at the Caltech Seismolab for information on the focal mechanisms for the M_l 3.5 Coso earthquake. We also thank Justin Rubinstein, Joan Gomberg, and two anonymous referees for constructive reviews. Z.P. and C.A. were supported by the National Science Foundation through awards EAR-0809834 and EAR-0956051.

References

Bhattacharyya, J., and J. M. Lees (2002), Seismicity and seismic stress in the Coso Range, Coso geothermal field, and Indian Wells Valley region, southeast-central California, *Mem. Geol. Soc. Am.*, *195*, 243–257.

Feng, Q., and J. M. Lees (1998), Microseismicity, stress, and fracture in the Coso geothermal field, California, *Tectonophysics*, *289*, 221–238, doi:10.1016/S0040-1951(97)00317-X.

Ghosh, A., J. E. Vidale, Z. Peng, K. C. Creager, and H. Houston (2009), Complex non-volcanic tremor near Parkfield triggered by the great 2004 Sumatra earthquake, *J. Geophys. Res.*, *114*, B00A15, doi:10.1029/2008JB006062.

Guilhem, A., Z. Peng, and R. M. Nadeau (2010), High-frequency identification of non-volcanic tremor along the San Andreas Fault triggered by regional earthquakes, *Geophys. Res. Lett.*, *37*, L16309, doi:10.1029/2010GL044660.

Hill, D. P. (2010), Surface wave potential for triggering tectonic (non-volcanic) tremor, *Bull. Seismol. Soc. Am.*, *100*, 1859–1878, doi:10.1785/0120090362.

Hill, D. P., and S. G. Prejean (2007), Dynamic triggering, in *Treatise on Geophysics*, vol. 4, *Earthquake Seismology*, edited by G. Schubert, pp. 257–292, Elsevier, Amsterdam.

Jiang, T., Z. Peng, W. Wang, and Q.-F. Chen (2010), Remotely triggered seismicity in continental China by the 2008 Mw7.9 Wenchuan earthquake, *Bull. Seismol. Soc. Am.*, *100*, 2574–2589, doi:10.1785/0120090286.

Kilb, D., J. Gomberg, and P. Bodin (2002), Aftershock triggering by complete Coulomb stress changes, *J. Geophys. Res.*, *107*(B4), 2060, doi:10.1029/2001JB000202.

Miyazawa, M., I. Nakanishi, Y. Sudo, and T. Ohkura (2005), Dynamic response of frequent tremors at Aso volcano to teleseismic waves from the 1999 Chi-Chi, Taiwan earthquake, *J. Volcanol. Geotherm. Res.*, *147*, 173–186, doi:10.1016/j.jvolgeores.2005.03.012.

Nadeau, R. M., and A. Guilhem (2009), Nonvolcanic tremor and the 2003 San Simeon and 2004 Parkfield, California earthquakes, *Science*, *325*, 191–193, doi:10.1126/science.1174155.

Peng, Z., and J. Gomberg (2010), An integrated perspective of the continuum between earthquakes and slow-slip phenomena, *Nat. Geosci.*, *3*, 599–607, doi:10.1038/ngeo940.

Peng, Z., J. E. Vidale, A. G. Wech, R. M. Nadeau, and K. C. Creager (2009), Remote triggering of tremor along the San Andreas Fault in central California, *J. Geophys. Res.*, *114*, B00A06, doi:10.1029/2008JB006049.

Prejean, S. G., et al. (2004), Remotely triggered seismicity on the United States West Coast following the Mw 7.9 Denali Fault earthquake, *Bull. Seismol. Soc. Am.*, *94*, S348–S359.

Rubinstein, J. L., J. Gomberg, J. E. Vidale, A. G. Wech, H. Kao, K. C. Creager, and G. Rogers (2009), Seismic wave triggering of nonvolcanic tremor, episodic tremor and slip, and earthquakes on Vancouver Island, *J. Geophys. Res.*, *114*, B00A01, doi:10.1029/2008JB005875.

Shelly, D. R., and J. L. Hardebeck (2010), Precise tremor source locations and amplitude variations along the lower-crustal central San Andreas Fault, *Geophys. Res. Lett.*, *37*, L14301, doi:10.1029/2010GL043672.

Shelly, D. R., G. C. Beroza, and S. Ide (2007), Non-volcanic tremor and low-frequency earthquake swarms, *Nature*, *446*, 305–307, doi:10.1038/nature05666.

Townend, J., and M. D. Zoback (2004), Regional tectonic stress near the San Andreas Fault in central and northern California, *Geophys. Res. Lett.*, *31*, L15S11, doi:10.1029/2003GL018918.

Velasco, A. A., S. Hernandez, T. Parsons, and K. Pankow (2008), Global ubiquity of dynamic earthquake triggering, *Nat. Geosci.*, *1*, 375–379, doi:10.1038/ngeo204.

C. Aiken and Z. Peng, School of Earth and Atmospheric Sciences, Georgia Institute of Technology, Atlanta, GA 30332, USA.

D. P. Hill and D. R. Shelly, U.S. Geological Survey, 345 Middlefield Rd., Menlo Park, CA 94025, USA.